CHEMISTRY OF MATERIALS
Cite This: Chem. Mater. 2018, 30, 5194−5204
Article
pubs.acs.org/cm

Mixed A-Cation Perovskites for Solar Cells: Atomic-Scale Insights Into Structural Distortion, Hydrogen Bonding, and Electronic Properties

Dibyajyoti Ghosh,[†,‡] Alexander R. Smith,[†] Alison B. Walker,[*,†] and M. Saiful Islam[*,‡]

[†]Department of Physics, University of Bath, Bath BA2 7AY, United Kingdom
[‡]Department of Chemistry, University of Bath, Bath BA2 7AY, United Kingdom

Supporting Information

ABSTRACT: Hybrid lead halide perovskites containing a mixture of A-site cations such as the formamidinium ($CH(NH_2)_2^+$, FA) and the smaller cesium (Cs^+) cations have attracted considerable interest due to their improved stability and solar cell performance. However, the structural changes at the atomic scale and modifications to the optoelectronic properties of these mixed cation perovskites are not fully understood. Here, we investigate the $FA_{1-x}Cs_xPbI_3$ ($x \leq 0.25$) system using a combination of static and dynamic *ab initio* computational methods. We find that the incorporation of Cs^+ cations into the parent $FAPbI_3$ structure induces a chemical pressure or lattice strain effect through Cs/FA ion size mismatch resulting in structural distortion and stronger FA-iodide (N−H···I) hydrogen bonding interactions. The dynamic tilting of PbI_6 octahedra and the rotational motion of FA cations are also suppressed, which leads to symmetry-breaking of the lattice. Such symmetry-breaking distortions of the Pb/I lattice give rise to a Rashba-type effect, which spin-splits the frontier electronic bands making the band gap indirect. Our results suggest that the direct−indirect band gap transition may be a factor in the reduced charge-carrier recombination rate in these mixed cation perovskites.

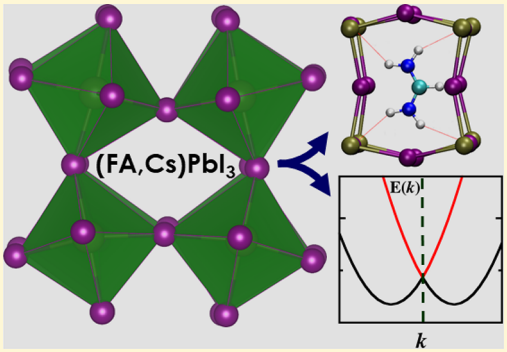

1. INTRODUCTION

Lead halide perovskite solar cells have shown a remarkable rise in power conversion efficiency from 3.8% to over 22% in less than a decade.[1−9] Along with their solution-processed fabrication, they possess many suitable properties for solar absorbers, including long charge-carrier lifetimes, a tunable band gap by cation or halide substitution, and compatibility with a wide range of charge collecting layers.

Despite their promising properties, a number of challenges need to be overcome before perovskite-based solar cell devices can be commercialized. Long-term stability at ambient conditions is one of the most important issues.[10−14] Compositional engineering has recently emerged as a potential approach to deliver higher stability without sacrificing power efficiency.[15−32]

Lead halide perovskites typically have the composition $APbX_3$ with the A-site occupied by a monovalent organic or inorganic cation (e.g., methylammonium $CH_3NH_3^+$ (MA^+), formamidinium $CH(NH_2)_2^+$ (FA^+), or cesium Cs^+) and the X-site by a halide anion (I^-, Br^-, or Cl^-). The PbX_3 component forms a framework cage of corner-sharing octahedra (shown in Figure 1) with the A-site cation (termed A-cation hereafter) at the center of each cage. Among compositional engineering approaches, the mixing of different sized A-cations has shown promise in producing longer lived solar cells.[17−22,24−28,33] In particular, partial substitution (of up to 25%) of FA cations by the much smaller Cs cations in $FAPbI_3$ stabilizes the perovskite phase against phase transitions and chemical degradation.[18,20,21,28,33,34] These mixed FA/Cs perovskites also exhibit improved optoelectronic properties, such as a tuned band gap,[18] enhanced charge-carrier mobility[20] and recombination lifetime,[20] and reduced energetic disordering.[18] As the static and dynamical structures influence these properties, it has been suggested that A-cation mixing modifies the internal interactions between the octahedral inorganic framework and organic cations. Despite a number of experimental reports and intriguing proposals, an in-depth atomistic understanding of these improvements is currently unclear.

We have carried out a range of recent studies on hybrid halide perovskites including work on ion transport, degradation, and defect passivation.[14,35−42] Here, we extend our previous work by investigating the structural distortions and interatomic interactions between the organic cations and inorganic framework of $FA_{1-x}Cs_xPbI_3$ ($x \leq 0.25$). Insights into the atomic-scale dynamical processes of the PbI framework and the organic cations are also provided by *ab initio* molecular dynamics simulations. The impact of A-cation mixing on the photovoltaic behavior and possible Rashba-type effects has

Received: May 4, 2018
Revised: July 2, 2018
Published: July 9, 2018

DOI: 10.1021/acs.chemmater.8b01851
Chem. Mater. 2018, 30, 5194−5204

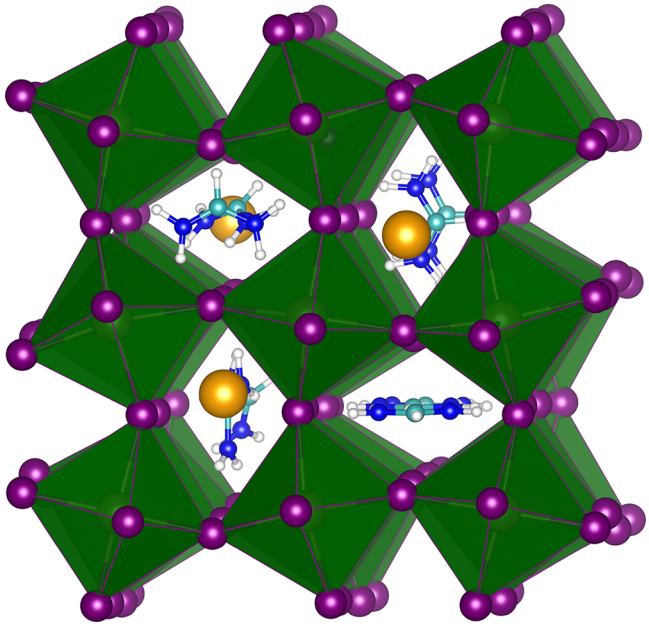

Figure 1. Schematic structure of a mixed A-cation metal halide perovskite. The A cations, FA^+ and Cs^+, occupy the inorganic cavity formed by corner-sharing PbI_6 octahedra (green). Key: iodine, purple; hydrogen, white; carbon, cyan; nitrogen, blue; cesium, orange.

been investigated by exploring electronic properties of these perovskites.

2. METHODS

Ab initio simulations were performed within the framework of density functional theory (DFT) as implemented in the Vienna Ab Initio Simulation Package (VASP)[43,44] using the Perdew–Burke–Ernzerhof functional for solids (PBEsol) within the generalized gradient approximation (GGA).[45,46] The projected augmented wave (PAW)[47] method and a plane-wave cutoff energy of 500 eV were employed for all the calculations. To simulate the impact of Cs incorporation with experimental concentrations of up to 25%,[20,33] a sufficiently large 4 × 4 × 4 supercell (64 A-cations) of the parent $FAPbI_3$ was chosen. We stress the necessity of a large structural supercell to model the experimental compositions for mixed A-cations. The extensive configuration space of cation distributions makes the *ab initio* computational investigations extremely challenging. Geometry relaxation was performed with *k*-point sampling at the Γ point, and the interatomic forces were relaxed with the convergence criteria of 0.01 eV $Å^{-1}$. A 3 × 3 × 3 Γ-centered Monkhorst–Pack sampling mesh with a Gaussian smearing of 0.01 eV was used for the electronic structure evaluation. To introduce a spin–orbit coupling (SOC) correction, geometry optimized 2 × 2 × 2 supercells of selective systems were considered. A 5 × 5 × 5 Γ-centered mesh was considered for the SOC-corrected electronic structure calculations.

To consider various possible conformations of FA^+ cations in $FAPbI_3$, the structural optimizations were initiated from up to 40 randomly generated geometries. We find that different orientations of the FA^+ cations result in small changes in total ground-state energy

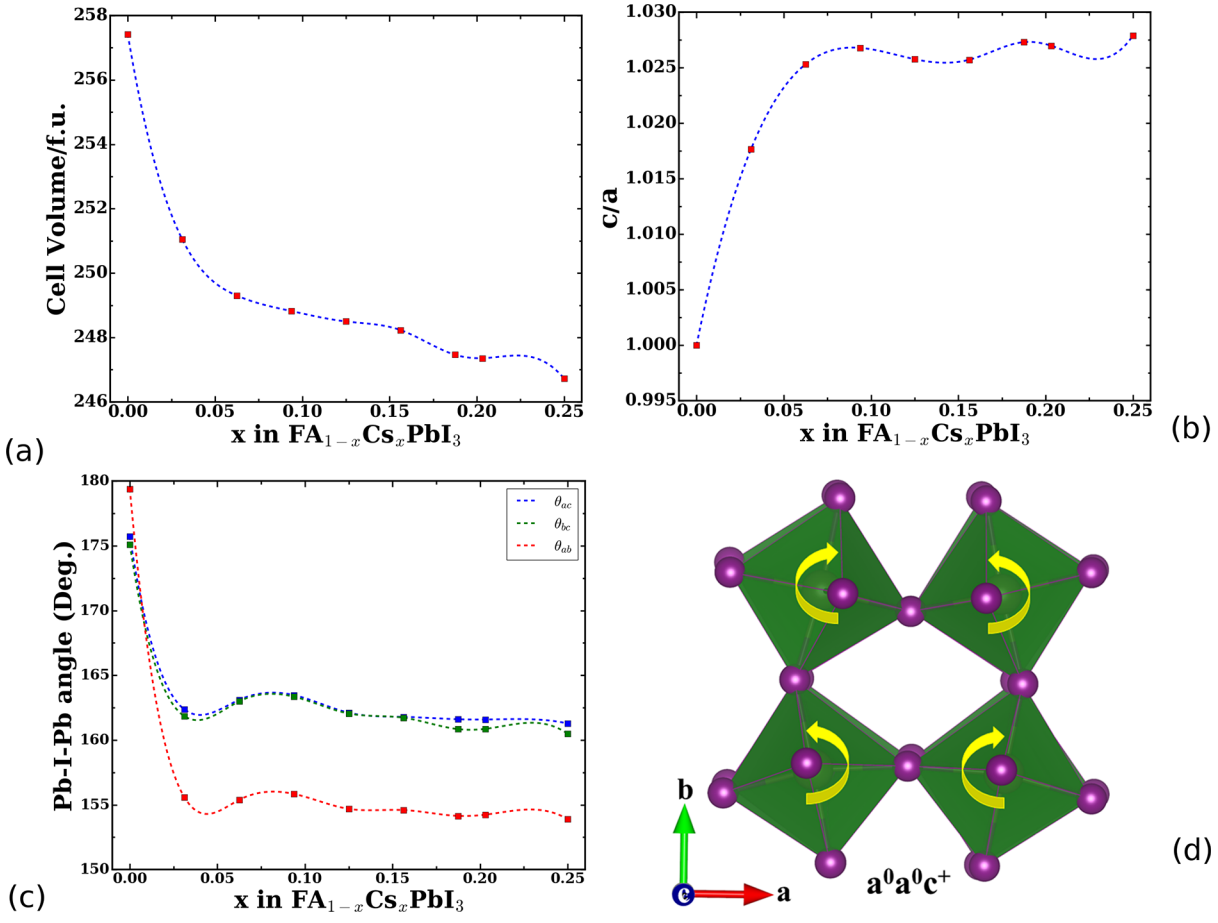

Figure 2. Structural distortion in $FA_{1-x}Cs_xPbI_3$. (a) Cell volume per formula unit, (b) c/a ratio, and (c) average Pb–I–Pb angle in three planes. (d) Tilting of PbI_6 octahedra with mutual in-phase rotation, i.e., $a^0a^0c^+$ in Glazer's notation for $FA_{0.85}Cs_{0.15}PbI_3$. Yellow arrows indicate the direction of rigid rotation of the octahedra.

DOI: 10.1021/acs.chemmater.8b01851
Chem. Mater. 2018, 30, 5194–5204

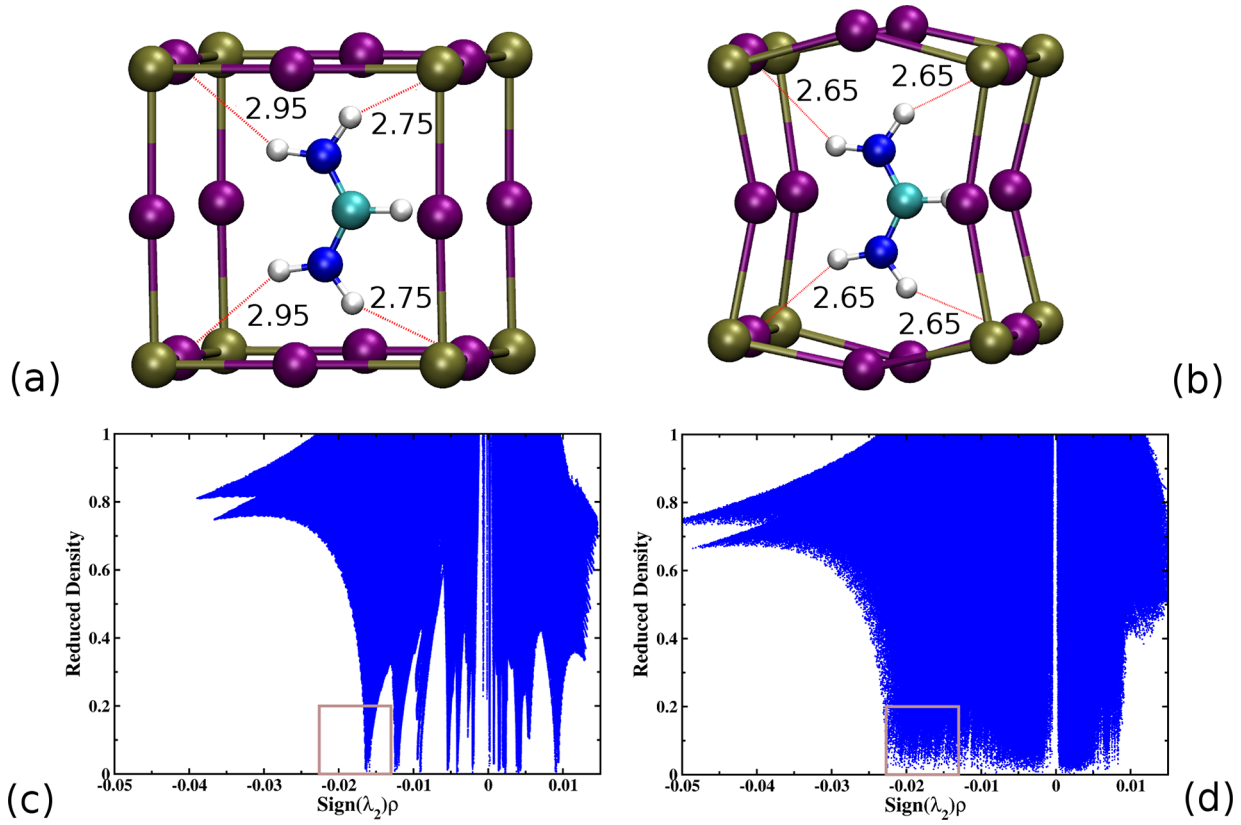

Figure 3. Enhanced hydrogen bonding with A-cation mixing. Schematic structures of H_N···I hydrogen bonds (red dashed lines) in (a) $FAPbI_3$ and (b) $FA_{0.85}Cs_{0.15}PbI_3$ with average bond lengths in Angstrom (Å). Reduced density gradient (s) plot as a function of Sign(λ_2)ρ for (c) $FAPbI_3$ and (d) $FA_{0.85}Cs_{0.15}PbI_3$. The brown boxes denote the range $-0.022 < \rho < -0.012$ where the hydrogen bonding mediated troughs are markedly different between $FAPbI_3$ and $FA_{0.85}Cs_{0.15}PbI_3$.

and lattice parameters. By exploring the configurational space for the mixed A-cation system $FA_{0.85}Cs_{0.15}PbI_3$, the highly dispersed Cs cation arrangements produced the lowest energy geometries, and such a cation distribution has been considered in this study (see Supporting Information (SI) for further details).

To investigate finite temperature effects, we also performed *ab initio* molecular dynamics simulations at 300 K using the CP2K package.[48] The QUICKSTEP formalism,[49] analytical dual-space pseudopotentials,[50] the GGA of the PBEsol form, and dispersion corrections as prescribed by Grimme (DFT-D3)[51] were used. Equilibrium dynamics were maintained in the NPT ensemble using a Nose-Hoover thermostat and a barostat as formulated by Martyna et al.[52] With a time step of 1 fs, each simulation covered a period of 40 ps, with the equilibration spanning the first 5 ps.

3. RESULTS AND DISCUSSION

3.1. Structural Distortion of the Perovskite Lattice. Simulations of the perovskite structures indicate that the lattice volume of $FA_{1-x}Cs_xPbI_3$ ($x \leq 0.25$) reduces with increasing Cs^+ content (Figure 2a), which is in agreement with X-ray diffraction studies.[21,33] The reduction of the unit cell volume in these mixed A-cation perovskites indicates chemical pressure effects, which relate to the internal structural contraction induced by the ion size mismatch between FA^+ (2.53 Å) and much smaller Cs^+ (1.67 Å).[53] Because of the soft mechanical nature of hybrid perovskites (with a bulk modulus <18 GPa[54,55]), such effects can be tuned by mixing the large and small sized A-cations in controlled proportions. These structural perturbations are expected to have prominent effects on their phase transitions,[56] solubility of ions in solid solutions,[18] and optoelectronic properties.[54]

By substituting small sized Cs^+ cations in place of FA^+, the parent cubic lattice contracts anisotropically and lowers the crystal symmetry to a tetragonal phase. The *a* and *b* lattice parameters contract, whereas the *c* lattice parameter elongates, increasing the *c*/*a* ratio by 2.8% (Figure 2b). This structural change leads to symmetry-reducing tetragonal distortion in the $FA_{1-x}Cs_xPbI_3$ lattice upon A-cation mixing.

The main source of the anisotropic volume contraction could be either the reduced internal volume of the PbI_6 octahedra with compressed Pb−I bonds and/or the octahedral tilting of corner-sharing PbI_6. To investigate both possibilities, we analyze (1) the average PbI_6 octahedral volume and the Pb−I bond distances, which indicate the distortion inside the octahedra, and (2) Pb−I−Pb angles, which represent the magnitude of the octahedral tilting. We find that the average PbI_6 volume and Pb−I bond lengths (Figure S3 a,b) remain unchanged upon A-cation mixing. Thus, A-cation mixing keeps the internal structure of PbI_6 octahedra unaltered. Interestingly, this contrasts with the tin-based system $FA_{1-x}Cs_xSnI_3$, where the Sn−I bond contracts with Cs^+ incorporation.[33]

Our results indicate that the average Pb−I−Pb angles decrease along with the lattice contraction of $FA_{1-x}Cs_xPbI_3$ (shown in Figure 2c). Specifically, with increasing Cs^+ concentration, the Pb−I−Pb bond angles are more strongly reduced in the *ab*-plane (θ_{ab}) than in the other planes (θ_{bc} and θ_{ac}), indicating rotation of PbI_6 octahedra about the *c*-axis. As shown in Figure 2d, adjacent PbI_6 octahedra tilt in the same direction, that is, "in-phase" about the *c*-axis.[33] Using Glazer

DOI: 10.1021/acs.chemmater.8b01851
Chem. Mater. 2018, 30, 5194−5204

notation,[57] such one-tilt rotations of octahedra are denoted $a^0a^0c^+$.

Therefore, as a consequence of the FA/Cs ion size mismatch, the cell volume contracts by tilting the PbI_6 octahedra. In a similar manner, applying low hydrostatic pressure (<5 GPa) has also been found to induce similar octahedral tilting based distortions and phase transitions in other hybrid perovskites including $MAPbI_3$ and $FAPbI_3$.[58−60] Tilting of corner-sharing octahedra is a relatively low-energy process[58,59,61] in these hybrid lead perovskites, and consequently, it becomes the source of structural distortion under weak perturbations such as cation substitution and mild external pressure.

3.2. Effect of H-Bonding. Lattice distortions can also modify the hydrogen bonding interactions between FA^+ cations and the PbI framework as discussed in our previous study.[36] By analyzing the $H_N\cdots I$ bonds in $FAPbI_3$, we find the shortest distances are 2.75 and 2.95 Å (see Figure 3a). In contrast, on incorporation of Cs, as in $FA_{0.85}Cs_{0.15}PbI_3$, all four $H_N\cdots I$ hydrogen bonds become much stronger due to the structural distortions (Figure 3b). As shown in Figure 3b, all the $H_N\cdots I$ distances are now ∼2.65 Å, which are shorter than that in the parent $FAPbI_3$.

To evaluate the strength of hydrogen bonding in $FA_{1-x}Cs_xPbI_3$, we perform an analysis based on the noncovalent interactions (NCI) index formulated by Johnson et al.[62,63] This analysis uses the electron density and its spatial derivatives to identify the noncovalent bonds in materials including the hybrid perovskites.[64,65] We analyze the reduced electron density gradient, s, as a function of $\mathrm{Sign}(\lambda_2)\rho$, where ρ and λ_2 are the electron density and the second eigenvalue of the electron density Hessian (second derivative) matrix, respectively (Figure 3c,d).[63] From this analysis, the appearance of troughs and singularities in $s(\rho)$ indicate the presence of noncovalent interactions. The sign of λ_2 denotes the type of interaction: for $\lambda_2 < 0$, the interaction is attractive (such as hydrogen bonding), whereas in the case of $\lambda_2 > 0$ it is repulsive (steric crowding). The interaction strength is determined by the density ρ; the higher the absolute value of ρ the stronger is the interaction.

As shown in Figure 3c,d, a greater number of troughs appear in the range $-0.022 < \rho < -0.012$ for $FA_{0.85}Cs_{0.15}PbI_3$ than for $FAPbI_3$. The troughs also move to a higher negative value of ρ in the mixed A-cation lattice (Figure 3c,d). As the highlighted range of ρ in Figure 3c,d indicates the degree of hydrogen bonding,[63] these plots show a strengthening of this noncovalent bonding interaction in the mixed A-cation perovskite. Because of the structural distortion, H_N atoms of the FA cations become spatially constrained and closer to the iodide anions, enhancing the strength of $H_N\cdots I$ hydrogen bonding interactions.

The stronger hydrogen bonding between molecular cations and the Pb/I lattice increases the internal energy of the perovskite phase. This is confirmed by the calculation of a favorable Helmholtz free energy of mixing for $FA_{0.85}Cs_{0.15}PbI_3$ of the order of 92 meV/formula unit at 300 K. In addition, we have examined the enthalpy of decomposition of both $FAPbI_3$ and $FA_{0.85}Cs_{0.15}PbI_3$ to PbI_2, FAI, and CsI and derived an exothermic value of −20 meV/formula unit and endothermic value of 135 meV/formula unit, respectively. We also find much weaker hydrogen bonding in the nonperovskite hexagonal phase of $FAPbI_3$ due to long $H_N\cdots I$ distances, with no significant change in hexagonal $FA_{1-x}Cs_xPbI_3$. This, in turn, correlates with the experimentally observed enhanced stability of the perovskite phase against the hexagonal phase for these mixed-cation halide perovskites[18,24,66] (see SI for details).

Hence, increased hydrogen bond strength helps to stabilize the structure and contributes to the greater thermal stability of the mixed A-cation perovskites. Similar phase stability induced by hydrogen bonding has also been observed for the low-temperature orthorhombic structure of $MAPbI_3$.[11,67−70] From computational work on $MAPbI_3$, Bristowe and Cheetham[64] suggest that tuning the degree of hydrogen bonding can also be used as an additional control parameter to optimize perovskite solar cell properties.

3.3. Dynamics of Inorganic Framework and Molecular A-Cations. A-cation mixing also affects the dynamic interactions and motion of the inorganic Pb/I cage and the organic cations.[36,71] We therefore performed *ab initio* molecular dynamics simulations of the parent $FAPbI_3$ and mixed A-cation system $FA_{0.85}Cs_{0.15}PbI_3$ at 300 K. First, considering the inorganic framework, we plot two-dimensional (2D) volumetric maps of a representative PbI frame in the *ab*-plane (Figure 4a,b). The 2D volumetric map represents the probability of atoms occupying positions in space over the time scale of the simulation. In Figure 4a, the iodine atoms of the parent $FAPbI_3$ show a symmetric distribution around the lattice sites, which are iodine lattice sites of the high-symmetry cubic structure. Thus, the time-averaged trajectories demonstrate an almost perfect cubic phase of $FAPbI_3$ (Figure 4a). In contrast, the 2D volumetric map for $FA_{0.85}Cs_{0.15}PbI_3$ (Figure 4b) shows significant spatial distribution of iodine atoms away from the cubic lattice sites. The time-averaged structure consequently clearly indicates the distorted low-symmetry lattice for $FA_{1-x}Cs_xPbI_3$.

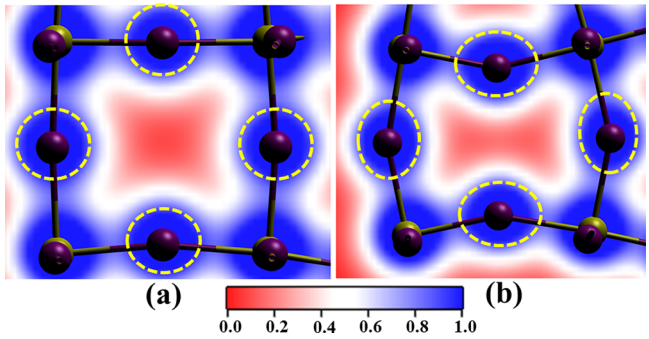

Figure 4. Dynamics of the inorganic framework in parent and mixed-cation perovskites. The volumetric plots of I and Pb atoms in a representative PbI-plane of (a) $FAPbI_3$ and (b) $FA_{0.85}Cs_{0.15}PbI_3$. This plot represents the number density of atoms in space over the simulation time. The scale is in arbitrary units, with blue and red indicating high and low number density, respectively. The ball−stick model of the inorganic framework shows the time-averaged positions of Pb and I atoms. The yellow dashed circles/ovals highlight the positions of iodine atoms over the simulation.

At room temperature, the iodide anions in $FAPbI_3$ oscillate about equilibrium positions in a regular cubic lattice with maximum displacements inside and outside of a cage due to periodic rotation of the octahedra about the pseudocubic axis.[36] As reported in recent inelastic X-ray scattering experiments and DFT-based computations, the energy barrier for octahedral tilting is only a few meV in these mechanically

DOI: 10.1021/acs.chemmater.8b01851
Chem. Mater. 2018, 30, 5194−5204

soft perovskites, and consequently, these oscillations are thermally active at room temperature.[61] However, our work shows that in $FA_{0.85}Cs_{0.15}PbI_3$ the iodide ions become constrained and oscillate through a smaller angle, with respect to their equilibrium positions either outside or inside of a PbI cage, suppressing low-energy vibrational modes. This constraining of the lattice inhibits the periodic rotational motion of PbI_6 octahedra about the *c*-axis at 300 K, locking the octahedra across the whole structure in a tilted geometry. The suppressed octahedral tilting motion in $FA_{1-x}Cs_xPbI_3$ causes a static octahedral distortion, which has recently been identified by X-ray diffraction studies of Prasanna et al.[33]

The molecular FA^+ cations also change their dynamic behavior upon Cs^+ incorporation. As illustrated in Figure 5a,

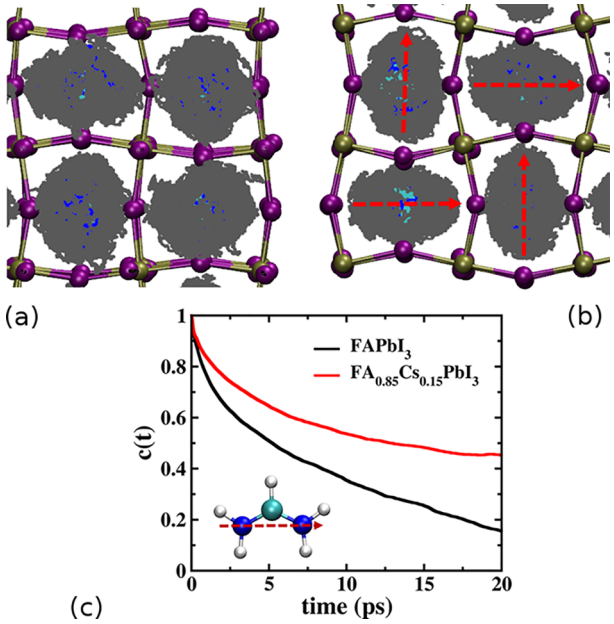

Figure 5. Dynamics of the FA^+ cation in parent and mixed-cation perovskites. The distribution of FA^+ cations in (a) $FAPbI_3$ and (b) $FA_{0.85}Cs_{0.15}PbI_3$ over the simulation time. The ball−stick model of the inorganic framework is the averaged position of Pb and I atoms over that time scale. Key: hydrogen, gray; carbon, cyan; nitrogen, blue. (c) Vector autocorrelation function of the FA^+ cation showing the probability of the cation remaining in its initial orientation over time. The molecular vectors of the FA^+ ion in b and the inset of c are represented by red dashed arrows.

the mobile FA cations in the parent $FAPbI_3$ explore full conformational space inside the inorganic cage showing no preferential orientation during the molecular dynamics simulation at 300 K. This disordered cation dynamics are in excellent agreement with quasi-elastic neutron scattering experiments, which also find a low barrier for reorientational motion inside the cage.[12,72] In contrast, for $FA_{0.85}Cs_{0.15}PbI_3$ the FA^+ cations exhibit constrained reorientational dynamics in which the N−N molecular axis preferentially aligns along the high-symmetry directions, [100] and [010] (Figure 5b). Furthermore, neighboring FA cations in the *ab*-crystal plane remain mutually perpendicular, orienting themselves along the elongated direction of the distorted cages (Figure 5b and Figure S4). Thus, the ordering of FA^+ cations is clearly influenced by the tetragonal distortion caused by the symmetry-lowering tilting of PbI_6 octahedra.

To further analyze the rotational motion of the FA^+ cations, we focus on the reorientation of the N−N molecular axis of the $CH(NH_2)_2^+$ cation (inset of Figure 5c) to capture the tumbling or "jump-like" rotation.[73] To obtain a quantitative description of this motion, we evaluate the vector autocorrelation function $c(t)$ of the N−N molecular axis from equilibrium trajectories. This function calculates the probability that the orientation of FA^+ cations remains directionally self-correlated over time. The faster the rotational correlation is lost, the faster the $c(t)$ decays with time.

As shown in Figure 5c, the autocorrelation function for tumbling rotation of FA^+ cations in $FAPbI_3$ decays much faster than that of $FA_{0.85}Cs_{0.15}PbI_3$. Notably, due to cation−lattice interactions, the FA^+ shows heterogeneous behavior in its dynamics in which the organic cation is inside the inorganic cage. We have therefore employed a stretched exponential fit to these autocorrelation functions to calculate the rotational relaxation time (see SI for details). We derive relaxation times for FA^+ reorientation of 8.8 and 28.2 ps (with exponent values β = 0.64 and 0.48) in $FAPbI_3$ and $FA_{0.85}Cs_{0.15}PbI_3$, respectively. The significant difference in relaxation times clearly indicates the restricted rotational dynamics of FA^+ cations at ambient conditions upon Cs^+ incorporation. Our simulated rotational relaxation time for FA^+ cations in $FAPbI_3$ matches well with a recent solid-state NMR study of Fabini et al.[74]

In summary, the lattice contraction and tetragonal distortion of the inorganic framework causes the spatial confinement of FA^+ cations, reducing the molecular tumbling dynamics at 300 K. Such restrained dynamics further increases the probability of the H_N atoms of $CH(NH_2)_2^+$ to reside closer to the electronegative iodide anions, enhancing the lattice−molecule interactions through stronger N−H···I hydrogen-bonding.[36] Since these effects reinforce each other, the reorientational modes of cation dynamics become restricted, causing partial immobilization of FA cations along [100] or [010] crystal axes at room temperature. Recently, the suppression of cation dynamics and formation of an orientational glassy phase have been observed by neutron scattering studies of $MA_{1-x}Cs_xPbBr_3$ perovskites.[71]

3.4. Effect on Electronic Properties. We now consider the electronic properties of $FA_{1-x}Cs_xPbI_3$ in relation to its photovoltaic behavior. As shown in Figure 6a, the band gap exhibits a blue-shift with increased Cs content from 1.52 eV (x = 0.06) to 1.59 eV (x = 0.25). Inclusion of spin−orbital coupling in the simulations strongly underestimates the band gap of $FA_{1-x}Cs_xPbI_3$ (Table S1), although the trend of variation with Cs concentration remains unchanged. This variation and increase in band gap values are in agreement with recent experimental absorption studies.[18,21,33] We note that due to the use of the semilocal exchange-correlation functional (PBEsol) the absolute band gap values have not been captured fully. The requirement for large simulation cell sizes prohibits us from applying a quasi-particle self-consistent GW approach with spin−orbit coupling corrections.[75] Nevertheless, as demonstrated in earlier studies,[76,77] we can still analyze the key trends in electronic properties and the impact of A-cation composition.

Along with the band gap, the relative energies and chemical bonding character of the band edges directly affect charge separation, influencing their efficiency as perovskite solar cell devices.[78,79] Applying the band-alignment scheme (see SI for details), the valence band maxima (VBM) downshift in energy

DOI: 10.1021/acs.chemmater.8b01851
Chem. Mater. 2018, 30, 5194−5204

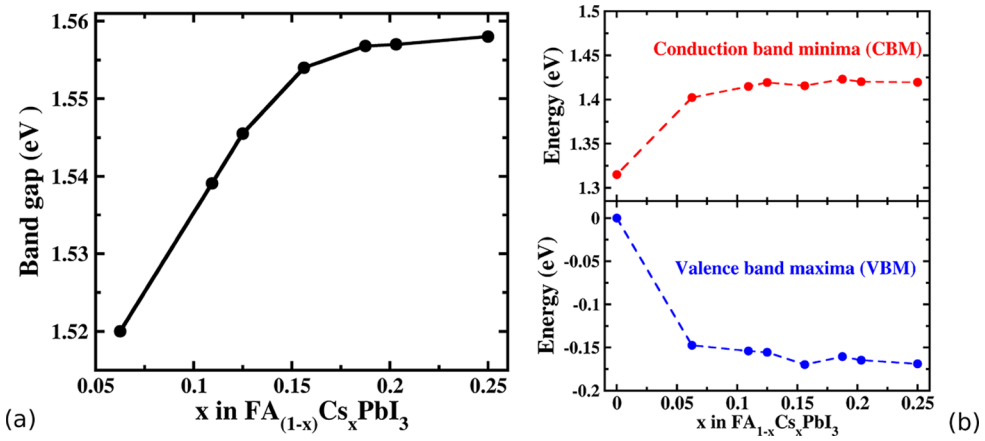

Figure 6. Electronic properties of $FA_{1-x}Cs_xPbI_3$ versus Cs concentration (x). (a) Variation in the band gap. (b) Variation in energy of conduction band minima (upper panel) and valence band maxima (lower panel). All energies are scaled to the VBM of $FAPbI_3$.

by 170 meV with increased Cs concentration, as shown in Figure 6(b). At the same time, the conduction band minima (CBM) shift upward in energy by a smaller amount of 100 meV. Overall, this leads to a blue-shift in the band gap, which is consistent with experimental absorption studies.[33] Note that inclusion of spin−orbit coupling does not change the overall trend in shifts of the band edges. We recognize that models based on band alignment have approximations. Nevertheless, the change in the band edges can tune the band offset between perovskite and charge transport layers, which may facilitate charge-carrier separation and transfer.[79]

To investigate the atomistic origin of the shift in energy level positions, we performed a detailed investigation of the chemical bonding nature of the CBM (Figure 7a,b) and VBM (Figure 7c,d). The charge density contours in Figure 7c,d show that the VBM originates from the antibonding overlap of Pb 6s and I 5p* orbitals, consistent with previous reports.[76,77] Furthermore, the site-projected density of states (pDOS, see Figure S5) indicate the covalent bonding nature of the VBM, in which 6s orbitals of Pb and 5p orbitals of I contribute ∼30−35% and ∼65−70%, respectively.

For cubic $FAPbI_3$, where the Pb−I−Pb alignment is almost linear, the antibonding orbital overlap in the VBM state remains significant (Figure 7c). With A-cation mixing, the in-phase PbI_6 octahedral tilting causes symmetry-lowering lattice distortion where the Pb−I−Pb bond angles deviate from 180° so that the I atoms are displaced out of the linear bonding geometry (see Figure 7d). This distortion reduces the energetically unfavorable antibonding overlap between Pb 6s and I 5p* orbitals, causing a decrease in the energy of the VBM of $FA_{1-x}Cs_xPbI_3$. Similar modification of the VBM across the structural phase transition of $FA_{1-x}Cs_xPbI_3$ has been reported from experimental spectroscopy studies.[33]

In contrast to the VBM, the CBM is dominated by Pb 6p nonbonding orbital contributions as shown in Figure 7b,d (see pDOS Figure S5). The localized nature of the electronic charge density indicates predominantly ionic character. Despite the nonbonding character, as shown in Figure 6b (upper panel), the CBM energy level is also influenced by A-cation mixing in these hybrid perovskites. The charge density contours of the CBM in $FAPbI_3$ and in the high Cs content system $FA_{0.75}Cs_{0.25}PbI_3$ (Figure 7a, b) show that A-cation mixing enhances the contribution of 5p-I orbitals to the conduction band, inducing partial covalent character. The

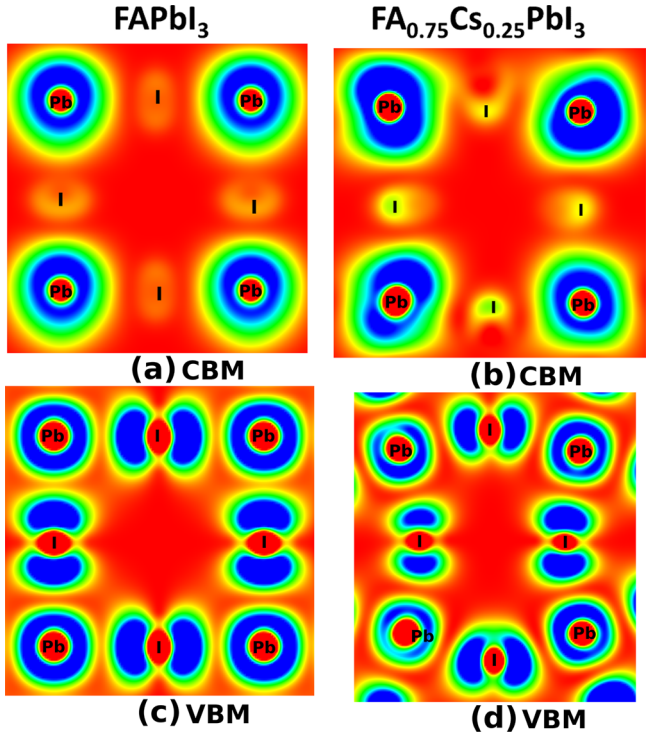

Figure 7. Electronic charge density contours. The conduction band minima (CBM) of (a) $FAPbI_3$ and (b) $FA_{0.75}Cs_{0.25}PbI_3$. The valence band maxima (VBM) of (c) $FAPbI_3$ and (d) $FA_{0.75}Cs_{0.25}PbI_3$. The CBM and VBM are dominated by the contributions from 6s orbitals of Pb and 5p orbitals of I. Color scale: red is defined as 0 and blue as 0.00015 $eÅ^{-3}$.

pDOS for the conduction band edge of $FA_{1-x}Cs_xPbI_3$ ($0 \leq x \leq 0.25$, Figure S6) also demonstrate the increased participation of 5p-I orbitals in this band with A-cation mixing. Such a variation in conduction band position with structural distortion is in line with previous computational studies on inorganic and hybrid lead halide perovskites.[64,76,77]

Because of the pseudo-Jahn−Teller effect, the symmetry-lowering distortion in the inorganic framework of $APbI_3$ perovskites increases the covalency of the Pb−I bond.[80] The increased covalent nature in the largely ionic CBM shifts the band to higher energy as shown in Figure 6b. Thus, A-cation mixing affects the VBM and CBM in opposing ways, leading to

DOI: 10.1021/acs.chemmater.8b01851
Chem. Mater. 2018, 30, 5194−5204

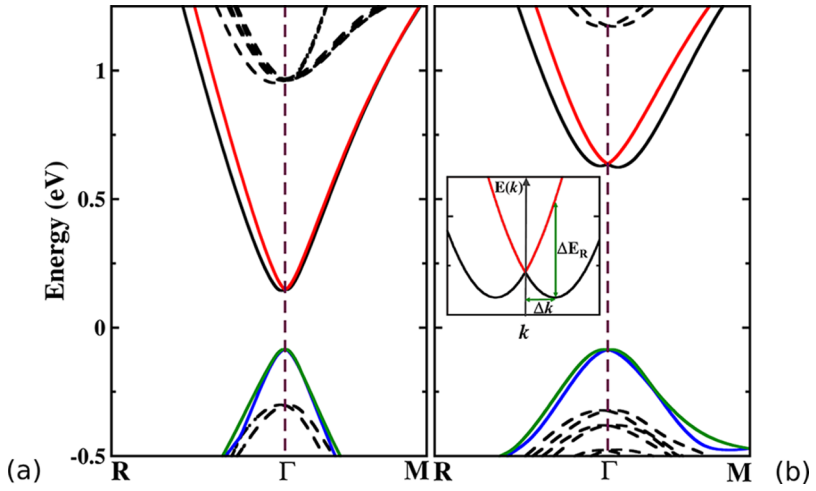

Figure 8. Rashba-type effect in mixed A-cation perovskites. The PBEsol-SOC electronic band structures of (a) $FAPbI_3$ and (b) $FA_{0.75}Cs_{0.25}PbI_3$. The Rashba−Dresselhaus splitting of the CBM in the M → Γ and R → Γ directions for $FA_{0.75}Cs_{0.25}PbI_3$ is prominent. Inset of b shows the zoomed section of the split conduction bands. The spin-split valence bands are shown in green and blue solid lines. The conduction bands are represented by black and red solid lines. All other bands are represented by dashed black lines.

an increase in the band gap. Recent X-ray and ultraviolet photoelectron spectroscopy experiments have also found a similar change in the energy levels in these mixed FA/Cs perovskites.[33]

As noted in previous studies, single A-cation perovskites such as $MAPbI_3$ can exhibit a Rashba-type effect where the spin degeneracies of the conduction and valence bands are lifted, which can also lead to an indirect band gap.[81−85] We now consider the structural distortions from FA/Cs ion size mismatch on possibly activating a Rashba-type spin-splitting[86,87] of the CBM and VBM, resulting in substantial modifications of the band edges of $FA_{1-x}Cs_xPbI_3$.[77,88] It is known that in the presence of heavy nuclei with high spin−orbit coupling constants, the Rashba-type effect spin-splits the band edges of materials which lack the local or extended inversion symmetry in their structure. To examine this effect, we have calculated band structures for $FAPbI_3$ and $FA_{0.75}Cs_{0.25}PbI_3$ as shown in Figure 8.

Along both the M → Γ and R → Γ directions, the ***k***-dependent spin-splitting of the conduction band shifts the band extrema from the high symmetry Γ-point for the mixed A-cation perovskite lattice. The momentum offset, Δ***k***, is the difference between the Γ-point and shifted band-extrema in *k*-space. For $FA_{0.75}Cs_{0.25}PbI_3$, Δ***k*** in the M → Γ and R → Γ high symmetry directions are 0.025 and 0.018 $Å^{-1}$, respectively. Δ***k*** for such splitting in its valence band is much lower with a value of only 0.001 $Å^{-1}$ along both directions. The differing extents of Δ***k*** in the frontier bands create an indirect band gap for $FA_{0.75}Cs_{0.25}PbI_3$ (see Table S1).

Fundamentally, the Rashba-type splitting is directly related to the strength of the spin−orbit coupling of elements. Hence, the conduction band, which is dominated by contributions from heavy Pb atoms (Figure 7a,b), splits more than the valence band in which the lighter I atoms largely contribute (Figure 7c,d). For $FAPbI_3$, however, the extent of spin-splitting in the conduction band along M → Γ and R → Γ directions (Figure 8a) is significantly lower than that in $FA_{0.75}Cs_{0.25}PbI_3$ (Figure 8b); in these two directions, Δ***k*** values for the conduction band in $FAPbI_3$ are only 0.002 and 0.003 $Å^{-1}$, respectively. Thus, considering static structures, the presence of greater symmetry-breaking distortion in mixed A-cation perovskites results in higher Rashba-type spin-splitting than that in $FAPbI_3$.

The strength of the Rashba-type effect can be represented by the parameter $\alpha = E_R/2\Delta k$, where E_R is the amplitude of the band splitting in a particular direction (see the inset of Figure 8c). In $FA_{0.75}Cs_{0.25}PbI_3$, the estimated α values in the M → Γ and R → Γ directions are 0.96 and 0.88 eV Å, respectively, which are of the same order as those reported by previous computational studies of related FA-iodide perovskites.[89]

Interestingly, several experimental reports based on time-correlated single-photon counting measurements have demonstrated an increased carrier lifetime for $FA_{1-x}Cs_xPb(I_{0.6}Br_{0.4})_3$ ($x \leq 0.25$).[18,20] Better crystallinity and removal of nonperovskite phases by A-cation mixing have been argued as the primary causes for the improved photovoltaic properties.[20] Our results suggest that changes in the static and dynamic interactions between the organic cation and inorganic Pb/I components in these mixed FA/Cs perovskites can also play an important role in the charge-carrier recombination.

As shown in Figure 8, structural distortions induce the Rashba-type spin-splitting of the band edges resulting in an indirect band gap in $FA_{0.75}Cs_{0.25}PbI_3$. As a consequence of the indirect nature of the band gap in these distorted perovskites, photogenerated carriers occupy the band extrema with different k-points in reciprocal space. This, in turn, may reduce the possibility of radiative electron−hole recombination, which is otherwise active in direct band gap semiconductors. In the radiative limit, an indirect band gap can affect the recombination rate for materials with low charge-carrier mobilities and smaller absorption coefficients for indirect over direct optical transitions.[90] Because of other complex factors such as defect densities and transitions from defect states, assessing the exact influence of an indirect band gap on nonradiative recombination rates is not straightforward and requires further in-depth study.

We have shown that structural distortion from FA/Cs ion size mismatch makes these mixed A-cation structures less dynamic and induces static symmetry-breaking. Hence, we suggest that under certain conditions static Rashba-type spin splitting can be a significant factor for charge-carrier recombination processes in these mixed A-cation perovskites.

DOI: 10.1021/acs.chemmater.8b01851
Chem. Mater. 2018, 30, 5194−5204

It should be noted that our finding of a static band-splitting mechanism is different from the recently demonstrated dynamical Rashba effect in $MAPbI_3$, which appears from dynamical local symmetry-breaking at finite temperatures.[91,92] We recognize that other influences on recombination have been considered in the much-studied $MAPbI_3$ including carrier trapping, polaronic screening, and an inverse absorption process.[40,93] Nevertheless, Rashba-type effects on the opto-electronic properties warrant further experimental studies as discussed by Stranks and Plochocka.[94] Such effects have also rendered hybrid perovskites as promising materials for spintronic applications.[88,94]

4. CONCLUSIONS

The changes in structural and optoelectronic properties of mixed A-site cation perovskite halides are not fully understood at the atomic scale. We have investigated the mixed cation system $FA_{1-x}Cs_xPbI_3$ using a combination of static and dynamic *ab initio* simulations with the following key features emerging: (a) Incorporation of Cs^+ cations into the parent $FAPbI_3$ compound induces significant structural distortion through ion size mismatch between the formamidinium ion ($CH(NH_2)_2^+$, FA^+) and the much smaller cesium ion (Cs^+). This results in octahedral tilting and stronger N−H···I hydrogen bonding between the organic FA cation and iodide ions (within the inorganic cages), which help to stabilize the structure and promote greater thermal stability. (b) We find that the dynamic tilting of PbI_6 octahedra and rotational motion of FA-cations are significantly inhibited in the mixed cation structure, which leads to static symmetry-breaking of the lattice. (c) The band gap can be tuned by compositional cation substitution. The calculated band gap is found to widen with increasing Cs content in $FA_{1-x}Cs_xPbI_3$ as observed experimentally. The alignment of frontier energy levels are also altered by the structural distortions. The symmetry-breaking distortions of the Pb/I lattice give rise to a Rashba-type effect, which spin-splits the frontier electronic bands making the band gap indirect. Our results suggest that the direct to indirect band gap transition may be a factor in the reduced rate of charge-carrier recombination in mixed A-cation perovskites.

These findings warrant further investigation and, indeed, one of the aims of our work is to stimulate new experimental studies in this area.

■ ASSOCIATED CONTENT

Supporting Information

The Supporting Information is available free of charge on the ACS Publications website at DOI: 10.1021/acs.chemmater.8b01851.

Detailed methods, phase stability, octahedral tilting, hydrogen bonding analysis, and reorientation relaxation time (PDF)

■ AUTHOR INFORMATION

Corresponding Authors

*(A.B.W.) E-mail: a.b.walker@bath.ac.uk.
*(M.S.I.) E-mail: m.s.islam@bath.ac.uk.

ORCID

Alison B. Walker: 0000-0002-2232-9734
M. Saiful Islam: 0000-0003-3882-0285

Notes

The authors declare no competing financial interest.

■ ACKNOWLEDGMENTS

This work was supported by the Energy oriented Centre of Excellence (EoCoE), grant agreement number 676629, funded within the Horizon2020 framework of the European Union. A.R.S. is supported by the EPSRC funded CDT in New and Sustainable Photovoltaics (reference EP/L01551X/1). M.S.I. and D.G. acknowledge support from the UK EPSRC Energy Materials Programme Grant (EP/K016288/1) and Archer HPC facilities through the Materials Chemistry Consortium (EP/L000202). We are grateful to Sam Stranks (Cambridge), Laurie Peter (Bath), Petra Cameron (Bath), and Juan Antonio Anta (Sevilla) for useful discussions.

■ REFERENCES

(1) Kojima, A.; Teshima, K.; Shirai, Y.; Miyasaka, T. Organometal Halide Perovskites as Visible-light Sensitizers for Photovoltaic Cells. *J. Am. Chem. Soc.* **2009**, *131*, 6050−6051.

(2) Lee, M. M.; Teuscher, J.; Miyasaka, T.; Murakami, T. N.; Snaith, H. J. Efficient Hybrid Solar Cells Based on Meso-superstructured Organometal Halide Perovskites. *Science* **2012**, *338*, 643−647.

(3) Green, M. A.; Ho-Baillie, A.; Snaith, H. J. The Emergence of Perovskite Solar Cells. *Nat. Photonics* **2014**, *8*, 506−514.

(4) Grätzel, M. The Light and Shade of Perovskite Solar Cells. *Nat. Mater.* **2014**, *13*, 838−842.

(5) Chen, W.; Wu, Y.; Yue, Y.; Liu, J.; Zhang, W.; Yang, X.; Chen, H.; Bi, E.; Ashraful, I.; Grätzel, M.; Han, L. Efficient and Stable Large-area Perovskite Solar Cells with Inorganic Charge Extraction Layers. *Science* **2015**, *350*, 944−948.

(6) Yang, W. S.; Noh, J. H.; Jeon, N. J.; Kim, Y. C.; Ryu, S.; Seo, J.; Seok, S. I. High-performance Photovoltaic Perovskite Layers Fabricated Through Intramolecular Exchange. *Science* **2015**, *348*, 1234−1237.

(7) Egger, D. A.; Rappe, A. M.; Kronik, L. Hybrid Organic−Inorganic Perovskites on the Move. *Acc. Chem. Res.* **2016**, *49*, 573−581.

(8) Correa-Baena, J.-P.; Abate, A.; Saliba, M.; Tress, W.; Jacobsson, T. J.; Grätzel, M.; Hagfeldt, A. The Rapid Evolution of Highly Efficient Perovskite Solar Cells. *Energy Environ. Sci.* **2017**, *10*, 710−727.

(9) Egger, D. A.; Bera, A.; Cahen, D.; Hodes, G.; Kirchartz, T.; Kronik, L.; Lovrincic, R.; Rappe, A. M.; Reichman, D. R.; Yaffe, O. What Remains Unexplained about the Properties of Halide Perovskites? *Adv. Mater.* **2018**, *30*, 1800691.

(10) Berhe, T. A.; Su, W.-N.; Chen, C.-H.; Pan, C.-J.; Cheng, J.-H.; Chen, H.-M.; Tsai, M.-C.; Chen, L.-Y.; Dubale, A. A.; Hwang, B.-J. Organometal Halide Perovskite Solar Cells: Degradation and Stability. *Energy Environ. Sci.* **2016**, *9*, 323−356.

(11) Stoumpos, C. C.; Malliakas, C. D.; Kanatzidis, M. G. Semiconducting tin and lead iodide perovskites with organic cations: Phase transitions, high mobilities, and near-infrared photoluminescent properties. *Inorg. Chem.* **2013**, *52*, 9019−9038.

(12) Chen, T.; Foley, B. J.; Park, C.; Brown, C. M.; Harriger, L. W.; Lee, J.; Ruff, J.; Yoon, M.; Choi, J. J.; Lee, S.-H. Entropy-driven Structural Transition and Kinetic Trapping in Formamidinium Lead Iodide Perovskite. *Sci. Adv.* **2016**, *2*, No. e1601650.

(13) Bryant, D.; Aristidou, N.; Pont, S.; Sanchez-Molina, I.; Chotchunangatchaval, T.; Wheeler, S.; Durrant, J. R.; Haque, S. A. Light and oxygen induced degradation limits the operational stability of methylammonium lead triiodide perovskite solar cells. *Energy Environ. Sci.* **2016**, *9*, 1655−1660.

(14) Aristidou, N.; Eames, C.; Sanchez-Molina, I.; Bu, X.; Kosco, J.; Islam, M. S.; Haque, S. A. Fast Oxygen Diffusion and Iodide Defects Mediate Oxygen-induced Degradation of Perovskite Solar Cells. *Nat. Commun.* **2017**, *8*, 15218.

DOI: 10.1021/acs.chemmater.8b01851
Chem. Mater. 2018, 30, 5194−5204

(15) Pellet, N.; Gao, P.; Gregori, G.; Yang, T.-Y.; Nazeeruddin, M. K.; Maier, J.; Grätzel, M. Mixed-organic-cation Perovskite photovoltaics for enhanced solar-light harvesting. *Angew. Chem., Int. Ed.* **2014**, *53*, 3151−3157.
(16) Jeon, N. J.; Noh, J. H.; Yang, W. S.; Kim, Y. C.; Ryu, S.; Seo, J.; Seok, S. I. Compositional Engineering of Perovskite Materials for High-performance Solar Cells. *Nature* **2015**, *517*, 476−480.
(17) Saliba, M.; Matsui, T.; Seo, J.-Y.; Domanski, K.; Correa-Baena, J.-P.; Mohammad, K. N.; Zakeeruddin, S. M.; Tress, W.; Abate, A.; Hagfeldt, A.; Grätzel, M. Cesium-containing Triple Cation Perovskite Solar Cells: Improved Stability, Reproducibility and High Efficiency. *Energy Environ. Sci.* **2016**, *9*, 1989−1997.
(18) McMeekin, D. P.; Sadoughi, G.; Rehman, W.; Eperon, G. E.; Saliba, M.; Hörantner, M. T.; Haghighirad, A.; Sakai, N.; Korte, L.; Rech, B.; Johnston, M. B.; Herz, L. M.; Snaith, H. J. A Mixed-cation Lead Mixed-halide Perovskite Absorber for Tandem Solar Cells. *Science* **2016**, *351*, 151−155.
(19) Niemann, R. G.; Gouda, L.; Hu, J.; Tirosh, S.; Gottesman, R.; Cameron, P. J.; Zaban, A. Cs^+ incorporation into $CH_3NH_3PbI_3$ perovskite: substitution limit and stability enhancement. *J. Mater. Chem. A* **2016**, *4*, 17819−17827.
(20) Rehman, W.; McMeekin, D. P.; Patel, J. B.; Milot, R. L.; Johnston, M. B.; Snaith, H. J.; Herz, L. M. Photovoltaic Mixed-cation Lead Mixed-halide Perovskites: Links between Crystallinity, Photostability and Electronic properties. *Energy Environ. Sci.* **2017**, *10*, 361−369.
(21) Lee, J.-W.; Kim, D.-H.; Kim, H.-S.; Seo, S.-W.; Cho, S. M.; Park, N.-G. Formamidinium and Cesium Hybridization for Photo-and Moisture-stable Perovskite Solar Cell. *Adv. Energy Mater.* **2015**, *5*, 1501310.
(22) Saliba, M.; Matsui, T.; Domanski, K.; Seo, J.-Y.; Ummadisingu, A.; Zakeeruddin, S. M.; Correa-Baena, J.-P.; Tress, W. R.; Abate, A.; Hagfeldt.; et al. Incorporation of Rubidium Cations into Perovskite Solar Cells Improves Photovoltaic Performance. *Science* **2016**, *354*, 206−209.
(23) Weber, O. J.; Charles, B.; Weller, M. T. Phase Behaviour and Composition in the Formamidinium-methylammonium Hybrid Lead Iodide Perovskite Solid Solution. *J. Mater. Chem. A* **2016**, *4*, 15375−15382.
(24) Yi, C.; Luo, J.; Meloni, S.; Boziki, A.; Ashari-Astani, N.; Grätzel, C.; Zakeeruddin, S. M.; Röthlisberger, U.; Grätzel, M. Entropic Stabilization of Mixed A-cation ABX_3 Metal Halide Perovskites for High Performance Perovskite Solar Cells. *Energy Environ. Sci.* **2016**, *9*, 656−662.
(25) Qiu, W.; Ray, A.; Jaysankar, M.; Merckx, T.; Bastos, J. P.; Cheyns, D.; Gehlhaar, R.; Poortmans, J.; Heremans, P. An interdiffusion method for highly performing cesium/formamidinium double cation perovskites. *Adv. Funct. Mater.* **2017**, *27*, 1700920.
(26) Bi, D.; Tress, W.; Dar, M. I.; Gao, P.; Luo, J.; Renevier, C.; Schenk, K.; Abate, A.; Giordano, F.; Baena, J.-P. C.; Decoppet.; et al. Efficient Luminescent Solar Cells Based on Tailored Mixed-cation Perovskites. *Sci. Adv.* **2016**, *2*, No. e1501170.
(27) Soufiani, A. M.; Yang, Z.; Young, T.; Miyata, A.; Surrente, A.; Pascoe, A.; Galkowski, K.; Abdi-Jalebi, M.; Brenes, R.; Urban, J.; et al. Impact of Microstructure on the Electron−hole Interaction in Lead Halide Perovskites. *Energy Environ. Sci.* **2017**, *10*, 1358−1366.
(28) Matsui, T.; Seo, J. Y.; Saliba, M.; Zakeeruddin, S. M.; Grätzel, M. Room Temperature Formation of Highly Crystalline Multication Perovskites for Efficient, Low-Cost Solar Cells. *Adv. Mater.* **2017**, *29*, 1606258.
(29) Duong, T.; Wu, Y.; Shen, H.; Peng, J.; Fu, X.; Jacobs, D.; Wang, E.-C.; Kho, T. C.; Fong, K. C.; Stocks.; et al. Rubidium Multication Perovskite with Optimized Bandgap for Perovskite-Silicon Tandem with over 26% Efficiency. *Adv. Energy Mater.* **2017**, *7*, 1700228.
(30) Singh, T.; Miyasaka, T. Stabilizing the efficiency beyond 20% with a mixed cation perovskite solar cell fabricated in ambient air under controlled humidity. *Adv. Funct. Mater.* **2018**, *8*, 1700677.
(31) Luo, P.; Zhou, S.; Zhou, Y.; Xia, W.; Sun, L.; Cheng, J.; Xu, C.; Lu, Y. Fabrication of Cs x FA1−x PbI3Mixed-Cation Perovskites via Gas-Phase-Assisted Compositional Modulation for Efficient and Stable Photovoltaic Devices. *ACS Appl. Mater. Interfaces* **2017**, *9*, 42708−42716.
(32) Zhang, X.; Liu, H.; Wang, W.; Zhang, J.; Xu, B.; Karen, K. L.; Zheng, Y.; Liu, S.; Chen, S.; Wang, K.; Sun, X. W. Hybrid Perovskite Light-Emitting Diodes Based on Perovskite Nanocrystals with Organic−Inorganic Mixed Cations. *Adv. Mater.* **2017**, *29*, 1606405.
(33) Prasanna, R.; Gold-Parker, A.; Leijtens, T.; Conings, B.; Babayigit, A.; Boyen, H.-G.; Toney, M. F.; McGehee, M. D. Band Gap Tuning via Lattice Contraction and Octahedral Tilting in Perovskite Materials for Photovoltaics. *J. Am. Chem. Soc.* **2017**, *139*, 11117−11124.
(34) Wang, Z.; McMeekin, D. P.; Sakai, N.; van Reenen, S.; Wojciechowski, K.; Patel, J. B.; Johnston, M. B.; Snaith, H. J. Efficient and Air-Stable Mixed-Cation Lead Mixed-Halide Perovskite Solar Cells with n-Doped Organic Electron Extraction Layers. *Adv. Mater.* **2017**, *29*, 1604186.
(35) Eames, C.; Frost, J. M.; Barnes, P. R.; O'regan, B. C.; Walsh, A.; Islam, M. S. Ionic Transport in Hybrid Lead Iodide Perovskite Solar Cells. *Nat. Commun.* **2015**, *6*, 7497.
(36) Ghosh, D.; Walsh Atkins, P.; Islam, M. S.; Walker, A. B.; Eames, C. Good Vibrations: Locking of Octahedral Tilting in Mixed-Cation Iodide Perovskites for Solar Cells. *ACS Energy Lett.* **2017**, *2*, 2424−2429.
(37) Charles, B.; Dillon, J.; Weber, O. J.; Islam, M. S.; Weller, M. T. Understanding the stability of mixed A-cation lead iodide perovskites. *J. Mater. Chem. A* **2017**, *5*, 22495−22499.
(38) Nagane, S.; Ghosh, D.; Hoye, R. L.; Zhao, B.; Ahmad, S.; Walker, A. B.; Islam, M. S.; Ogale, S.; Sadhanala, A. Lead-Free Perovskite Semiconductors Based on Germanium−Tin Solid Solutions: Structural and Optoelectronic Properties. *J. Phys. Chem. C* **2018**, *122*, 5940−5947.
(39) Pering, S. R.; Deng, W.; Troughton, J. R.; Kubiak, P.; Ghosh, D.; Niemann, R.; Brivio, F.; Jeffrey, F.; Walker, A.; Islam, M.; et al. Azetidinium lead iodide for perovskite solar cells. *J. Mater. Chem. A* **2017**, *5*, 20658−20665.
(40) Brenes, R.; Eames, C.; Bulović, V.; Islam, M. S.; Stranks, S. D. The Impact of Atmosphere on the Local Luminescence Properties of Metal Halide Perovskite Grains. *Adv. Mater.* **2018**, *30*, 1706208.
(41) Brenes, R.; Guo, D.; Osherov, A.; Noel, N. K.; Eames, C.; Hutter, E. M.; Pathak, S. K.; Niroui, F.; Friend, R. H.; Islam, M. S. a.; et al. Metal Halide Perovskite Polycrystalline Films Exhibiting Properties of Single Crystals. *Joule* **2017**, *1*, 155−167.
(42) Dawson, J. A.; Naylor, A. J.; Eames, C.; Roberts, M.; Zhang, W.; Snaith, H. J.; Bruce, P. G.; Islam, M. S. Mechanisms of lithium intercalation and conversion processes in organic−inorganic halide perovskites. *ACS Energy Lett.* **2017**, *2*, 1818−1824.
(43) Kresse, G.; Hafner, J. Ab initio molecular dynamics for liquid metals. *Phys. Rev. B: Condens. Matter Mater. Phys.* **1993**, *47*, 558.
(44) Kresse, G.; Hafner, J. Ab initio molecular-dynamics simulation of the liquid-metal−amorphous-semiconductor transition in germanium. *Phys. Rev. B: Condens. Matter Mater. Phys.* **1994**, *49*, 14251.
(45) Perdew, J. P.; Burke, K.; Ernzerhof, M. Generalized Gradient Approximation Made Simple. *Phys. Rev. Lett.* **1996**, *77*, 3865.
(46) Perdew, J. P.; Ruzsinszky, A.; Csonka, G. I.; Vydrov, O. A.; Scuseria, G. E.; Constantin, L. A.; Zhou, X.; Burke, K. Restoring the density-gradient expansion for exchange in solids and surfaces. *Phys. Rev. Lett.* **2008**, *100*, 136406.
(47) Kresse, G.; Joubert, D. From ultrasoft pseudopotentials to the projector augmented-wave method. *Phys. Rev. B: Condens. Matter Mater. Phys.* **1999**, *59*, 1758.
(48) Hutter, J.; Iannuzzi, M.; Schiffmann, F.; VandeVondele, J. CP2K: Atomistic Simulations of Condensed Matter Systems. *Wiley Interdiscip. Rev. Comput. Mol. Sci.* **2014**, *4*, 15−25.
(49) VandeVondele, J.; Krack, M.; Mohamed, F.; Parrinello, M.; Chassaing, T.; Hutter, J. Quickstep: Fast and Accurate Density Functional Calculations using a Mixed Gaussian and Plane Waves Approach. *Comput. Phys. Commun.* **2005**, *167*, 103−128.

DOI: 10.1021/acs.chemmater.8b01851
Chem. Mater. 2018, 30, 5194−5204

(50) Hartwigsen, C.; Gœdecker, S.; Hutter, J. Relativistic separable dual-space Gaussian pseudopotentials from H to Rn. *Phys. Rev. B: Condens. Matter Mater. Phys.* **1998**, *58*, 3641.
(51) Grimme, S. Semiempirical GGA-type Density Functional Constructed with a Long-range Dispersion Correction. *J. Comput. Chem.* **2006**, *27*, 1787−1799.
(52) Martyna, G. J.; Tobias, D. J.; Klein, M. L. Constant Pressure Molecular Dynamics Algorithms. *J. Chem. Phys.* **1994**, *101*, 4177−4189.
(53) Kieslich, G.; Sun, S.; Cheetham, A. K. Solid-state principles applied to organic−inorganic perovskites: new tricks for an old dog. *Chem. Sci.* **2014**, *5*, 4712−4715.
(54) Jaffe, A.; Lin, Y.; Karunadasa, H. I. Halide Perovskites Under Pressure: Accessing New Properties Through Lattice Compression. *ACS Energy Lett.* **2017**, *2*, 1549−1555.
(55) Wang, L.; Wang, K.; Zou, B. Pressure-induced structural and optical properties of organometal halide perovskite-based formamidinium lead bromide. *J. Phys. Chem. Lett.* **2016**, *7*, 2556−2562.
(56) Gratia, P.; Zimmermann, I.; Schouwink, P.; Yum, J.-H.; Audinot, J.-N.; Sivula, K.; Wirtz, T.; Nazeeruddin, M. K. The Many Faces of Mixed Ion Perovskites: Unraveling and Understanding the Crystallization Process. *ACS Energy Lett.* **2017**, *2*, 2686−2693.
(57) Glazer, A. The Classification of Tilted Octahedra in Perovskites. *Acta Crystallogr., Sect. B: Struct. Crystallogr. Cryst. Chem.* **1972**, *28*, 3384−3392.
(58) Szafranski, M.; Katrusiak, A. Mechanism of pressure-induced phase transitions, amorphization, and absorption-edge shift in photovoltaic methylammonium lead iodide. *J. Phys. Chem. Lett.* **2016**, *7*, 3458−3466.
(59) Jiang, S.; Fang, Y.; Li, R.; Xiao, H.; Crowley, J.; Wang, C.; White, T. J.; Goddard, W. A.; Wang, Z.; Baikie, T.; Fang, J. Pressure-Dependent Polymorphism and Band-Gap Tuning of Methylammonium Lead Iodide Perovskite. *Angew. Chem., Int. Ed.* **2016**, *55*, 6540−6544.
(60) Wang, P.; Guan, J.; Galeschuk, D. T.; Yao, Y.; He, C. F.; Jiang, S.; Zhang, S.; Liu, Y.; Jin, M.; Jin, C.; Soong, Y. Pressure-Induced Polymorphic, Optical, and Electronic Transitions of Formamidinium Lead Iodide Perovskite. *J. Phys. Chem. Lett.* **2017**, *8*, 2119−2125.
(61) Beecher, A. N.; Semonin, O. E.; Skelton, J. M.; Frost, J. M.; Terban, M. W.; Zhai, H.; Alatas, A.; Owen, J. S.; Walsh, A.; Billinge, S. J. Direct observation of dynamic symmetry breaking above room temperature in methylammonium lead iodide perovskite. *ACS Energy Lett.* **2016**, *1*, 880−887.
(62) Johnson, E. R.; Keinan, S.; Mori-Sanchez, P.; Contreras-Garcia, J.; Cohen, A. J.; Yang, W. Revealing noncovalent interactions. *J. Am. Chem. Soc.* **2010**, *132*, 6498−6506.
(63) Contreras-García, J.; Johnson, E. R.; Keinan, S.; Chaudret, R.; Piquemal, J.-P.; Beratan, D. N.; Yang, W. NCIPLOT: a program for plotting noncovalent interaction regions. *J. Chem. Theory Comput.* **2011**, *7*, 625−632.
(64) Lee, J.-H.; Bristowe, N. C.; Lee, J. H.; Lee, S.-H.; Bristowe, P. D.; Cheetham, A. K.; Jang, H. M. Resolving the Physical Origin of Octahedral Tilting in Halide Perovskites. *Chem. Mater.* **2016**, *28*, 4259−4266.
(65) El-Mellouhi, F.; Marzouk, A.; Bentria, E. T.; Rashkeev, S. N.; Kais, S.; Alharbi, F. H. Hydrogen Bonding and Stability of Hybrid Organic−Inorganic Perovskites. *ChemSusChem* **2016**, *9*, 2648−2655.
(66) Niemann, R. G.; Gouda, L.; Hu, J.; Tirosh, S.; Gottesman, R.; Cameron, P. J.; Zaban, A. Cs^+ Incorporation Into $CH_3NH_3PbI_3$ Perovskite: Substitution Limit and Stability Enhancement. *J. Mater. Chem. A* **2016**, *4*, 17819.
(67) Weller, M. T.; Weber, O. J.; Henry, P. F.; Di Pumpo, M.; Hansen, T. C. Complete Structure and Cation Orientation in the Perovskite Photovoltaic Methylammonium Lead Iodide between 100 and 352 K. *Chem. Commun.* **2015**, *51*, 4180−4183.
(68) Lee, J.-H.; Bristowe, N. C.; Bristowe, P. D.; Cheetham, A. K. Role of hydrogen-bonding and its interplay with octahedral tilting in CH 3 NH 3 PbI 3. *Chem. Commun.* **2015**, *51*, 6434−6437.
(69) Poglitsch, A.; Weber, D. Dynamic disorder in methylammoniumtrihalogenoplumbates (II) observed by millimeter-wave spectroscopy. *J. Chem. Phys.* **1987**, *87*, 6373−6378.
(70) Lee, J. H.; Lee, J.-H.; Kong, E.-H.; Jang, H. M. The nature of hydrogen-bonding interaction in the prototypic hybrid halide perovskite, tetragonal CH 3 NH 3 PbI 3. *Sci. Rep.* **2016**, *6*, 21687.
(71) Mozur, E. M.; Maughan, A. E.; Cheng, Y.; Huq, A.; Jalarvo, N.; Daemen, L. L.; Neilson, J. R. Orientational Glass Formation in Substituted Hybrid Perovskites. *Chem. Mater.* **2017**, *29*, 10168−10177.
(72) Weller, M. T.; Weber, O. J.; Frost, J. M.; Walsh, A. Cubic perovskite structure of black formamidinium lead iodide, α-$[HC(NH_2)_2]PbI_3$, at 298 K. *J. Phys. Chem. Lett.* **2015**, *6*, 3209−3212.
(73) Bakulin, A. A.; Selig, O.; Bakker, H. J.; Rezus, Y. L.; Muller, C.; Glaser, T.; Lovrincic, R.; Sun, Z.; Chen, Z.; Walsh, A.; et al. Real-time observation of organic cation reorientation in methylammonium lead iodide perovskites. *J. Phys. Chem. Lett.* **2015**, *6*, 3663−3669.
(74) Fabini, D. H.; Siaw, T. A.; Stoumpos, C. C.; Laurita, G.; Olds, D.; Page, K.; Hu, J. G.; Kanatzidis, M. G.; Han, S.; Seshadri, R. Universal Dynamics of Molecular Reorientation in Hybrid Lead Iodide Perovskites. *J. Am. Chem. Soc.* **2017**, *139*, 16875−16884.
(75) Brivio, F.; Butler, K. T.; Walsh, A.; Van Schilfgaarde, M. Relativistic quasiparticle self-consistent electronic structure of hybrid halide perovskite photovoltaic absorbers. *Phys. Rev. B: Condens. Matter Mater. Phys.* **2014**, *89*, 155204.
(76) Meloni, S.; Palermo, G.; Ashari-Astani, N.; Grätzel, M.; Rothlisberger, U. Valence and conduction band tuning in halide perovskites for solar cell applications. *J. Mater. Chem. A* **2016**, *4*, 15997−16002.
(77) Amat, A.; Mosconi, E.; Ronca, E.; Quarti, C.; Umari, P.; Nazeeruddin, M. K.; Grätzel, M.; De Angelis, F. Cation-induced Band-gap Tuning in Organohalide Perovskites: Interplay of Spin−orbit Coupling and Octahedra Tilting. *Nano Lett.* **2014**, *14*, 3608−3616.
(78) Correa Baena, J. P.; Steier, L.; Tress, W.; Saliba, M.; Neutzner, S.; Matsui, T.; Giordano, F.; Jacobsson, T. J.; Kandada, A. R. S.; et al. Highly efficient planar perovskite solar cells through band alignment engineering. *Energy Environ. Sci.* **2015**, *8*, 2928−2934.
(79) Yin, W.-J.; Yang, J.-H.; Kang, J.; Yan, Y.; Wei, S.-H. Halide perovskite materials for solar cells: a theoretical review. *J. Mater. Chem. A* **2015**, *3*, 8926−8942.
(80) Garcia-Fernandez, P.; Aramburu, J.; Barriuso, M.; Moreno, M. Key role of covalent bonding in octahedral tilting in perovskites. *J. Phys. Chem. Lett.* **2010**, *1*, 647−651.
(81) Niesner, D.; Wilhelm, M.; Levchuk, I.; Osvet, A.; Shrestha, S.; Batentschuk, M.; Brabec, C.; Fauster, T. Giant rashba splitting in CH 3 NH 3 PbBr 3 organic-inorganic perovskite. *Phys. Rev. Lett.* **2016**, *117*, 126401.
(82) Wang, T.; Daiber, B.; Frost, J. M.; Mann, S. A.; Garnett, E. C.; Walsh, A.; Ehrler, B. Indirect to direct bandgap transition in methylammonium lead halide perovskite. *Energy Environ. Sci.* **2017**, *10*, 509−515.
(83) Hutter, E. M.; Gélvez-Rueda, M. C.; Osherov, A.; Bulović, V.; Grozema, F. C.; Stranks, S. D.; Savenije, T. J. Direct−indirect character of the bandgap in methylammonium lead iodide perovskite. *Nat. Mater.* **2017**, *16*, 115−120.
(84) Zhai, Y.; Baniya, S.; Zhang, C.; Li, J.; Haney, P.; Sheng, C.-X.; Ehrenfreund, E.; Vardeny, Z. V. Giant Rashba splitting in 2D organic-inorganic halide perovskites measured by transient spectroscopies. *Sci. Adv.* **2017**, *3*, No. e1700704.
(85) Zheng, F.; Tan, L. Z.; Liu, S.; Rappe, A. M. Rashba spin−orbit coupling enhanced carrier lifetime in CH3NH3PbI3. *Nano Lett.* **2015**, *15*, 7794−7800.
(86) Dresselhaus, G. Spin-orbit coupling effects in zinc blende structures. *Phys. Rev.* **1955**, *100*, 580.
(87) Rashba, E. Symmetry of energy bands in crystals of wurtzite type. 1. Symmetry of bands disregarding spin-orbit interaction. *Sov. Phys. Solid State* **1959**, *1*, 368−380.

DOI: 10.1021/acs.chemmater.8b01851
Chem. Mater. 2018, 30, 5194−5204

(88) Kepenekian, M.; Even, J. Rashba and Dresselhaus Couplings in Halide Perovskites: Accomplishments and Opportunities for Spintronics and Spin−Orbitronics. *J. Phys. Chem. Lett.* **2017**, *8*, 3362−3370.
(89) Stroppa, A.; Di Sante, D.; Barone, P.; Bokdam, M.; Kresse, G.; Franchini, C.; Whangbo, M.-H.; Picozzi, S. Tunable ferroelectric polarization and its interplay with spin−orbit coupling in tin iodide perovskites. *Nat. Commun.* **2014**, *5*, 5900.
(90) Kirchartz, T.; Rau, U. Decreasing radiative recombination coefficients via an indirect band gap in lead halide perovskites. *J. Phys. Chem. Lett.* **2017**, *8*, 1265−1271.
(91) Etienne, T.; Mosconi, E.; De Angelis, F. Dynamical origin of the rashba effect in organohalide lead perovskites: A key to suppressed carrier recombination in perovskite solar cells? *J. Phys. Chem. Lett.* **2016**, *7*, 1638−1645.
(92) Quarti, C.; Mosconi, E.; De Angelis, F. Interplay of orientational order and electronic structure in methylammonium lead iodide: implications for solar cell operation. *Chem. Mater.* **2014**, *26*, 6557−6569.
(93) Davies, C. L.; Filip, M. R.; Patel, J. B.; Crothers, T. W.; Verdi, C.; Wright, A. D.; Milot, R. L.; Giustino, F.; Johnston, M. B.; Herz, L. M. Bimolecular recombination in methylammonium lead triiodide perovskite is an inverse absorption process. *Nat. Commun.* **2018**, *9*, 293.
(94) Stranks, S. D.; Plochocka, P. The influence of the Rashba effect. *Nat. Mater.* **2018**, *17*, 381−382.

DOI: 10.1021/acs.chemmater.8b01851
Chem. Mater. 2018, 30, 5194−5204